CHAPTER 84

The Propagation of Water Waves in Prismatic Channels

Li Li[1], Robert A. Dalrymple[2] and Jeffrey M. Mlynarski[3]

Abstract:

Short waves in a channel can present navigational problems and may excite harbor oscillations. Channel sidewalls may reduce much of this wave energy, if they are sufficiently porous or they are sloped. Previously we presented a model for wave propagation in prismatic channels of arbitrary cross-section utilizing a numerical eigenfunction expansion. Here a series of small scale laboratory experiments were conducted to verify the numerical model. Comparisons of the numerical model to the experimental data are made for water surface profile and for eigenfunctions. The possibility of resonance between the edge wave and the second harmonic of the incident wave is also studied.

1 Introduction

Water waves encountering entrance channels present an interesting problem as the waves undergo reflection, refraction, diffraction and shoaling due to shorelines, shoals, jetties, tidal currents, and channels with varying depths. Long waves within channels have served as the impetus for the study of waves. Kelland (1839, as cited in Lamb, 1945) provided a wave equation for waves in triangular channels with the sidewalls inclined at 45°. Scott Russell (1844) provided evidence for the presence of solitary waves in channels. More recently, Peregrine (1968, 1969) examined nonlinear long waves in narrow channel. Golinko (1987) studied the reflection of a long wave from the vertical walls of a channel with a parabolic cross-section. Mathew and Akylas

[1]Graduate Student, Center for Applied Coastal Research, Department of Civil and Environment Engineering, University of Delaware, Newark, DE 19716, USA.

[2]Professor, Department of Civil and Environment Engineering, Center for Applied Coastal Research, University of Delaware, Newark, DE 19716, USA

[3]Student, Department of Civil and Environment Engineering, University of Delaware, Newark, DE 19716, USA

(1990) conducted research on the wide channel case, noting the three-dimensional nature of the waves. Teng and Wu (1994) studied nonlinear long wave in convergent and divergent channels.

However, short waves in a channel also can present navigational problems and may excite harbor oscillations, and less work has been done on short waves. Kelland (1839) and Macdonald (1894) (all cited in Lamb, 1945) obtained analytical solutions for triangular channels with the sidewalls inclined at 45° and 60° to the vertical. Recently, Isaacson (1978) studied wave decay along the center line of a trapezoidal channel with rubble sidewalls in a laboratory experiment. Melo and Guza (1991*a*, 1991*b*), through field and numerical means, showed that a tidal inlet comprised of rubblemound jetties absorbed a considerable amount of the wave energy entering the inlet from the ocean into the porous inlet sidewalls. Dalrymple (1992) developed a simple model to explain this behavior using a simple eigenfunction expansion of the waves in the channel (assuming a rectangular channel cross-section) and an impedance boundary condition at the sidewalls. It was assumed that the waves at the mouth of the inl et had a constant amplitude and phase; that is, they were planar and normally incident. One consequence of this assumption and the impedance boundary condition was a fictitious amplification of the waves occurring within one wavelength of the channel mouth. Dalrymple and Martin (1996) have reduced this amplification by including the effect of the scattering of waves into the ocean. Kirby, Dalrymple, Kaku (1994) used parabolic model to study conformal coordinate system. Dalrymple, Kirby, Martin (1994) used spectral model to study conformally-mapped channel, including the diverging channels and circular channels.

Dalrymple, Kirby and Li (1994) using an eigenfunction expansion, studied an arbitrary cross-section channel. The basis of the eigenfunction expansion model is that the wave motion can be viewed as a summation of simple eigenmodes (Y_n) in the cross-channel direction. The amplitudes of the eigenmodes (A_n) are determined at the mouth of the channel. The wave motion (in an assumed ideal fluid) is governed by the following equation:

$$\Phi(x,y,z,t) = \widehat{\phi}(x,y)\,\frac{\cosh k(h+z)}{\cosh kh}e^{-\mathrm{i}\omega t}$$

$$\widehat{\phi}(x,y) = \sum_{n=0}^{\infty} A_n\, e^{\mathrm{i}\sqrt{\overline{K^2}-\lambda_n^2}x} Y_n(y)$$

$$\frac{d^2Y}{dy^2} + \left(\lambda^2 - \overline{K^2}\,\nu(y)\right) Y = 0$$

where x is the propagation direction, y is the direction across the channel, z is the direction vertically upwards from the still water level, k is the local wavenumber, g is gravity; C and C_g are the phase and group velocity, corresponding the dispersion relationship, $\omega^2 = gk\tanh kh$.

Channels with symmetric and antisymmetric cross section were studied. With the numerical model, showed that channels with sloping sidewalls give rise to the presence of edge waves, excited by the incident wave field, while the incident wave propagate in the center of channel. The edge wave length is shorter than the incident wave

length. The edge wave amplitude, represented by the zeroth mode eigenfunction, is much higher than the magnitude of the incident wave.

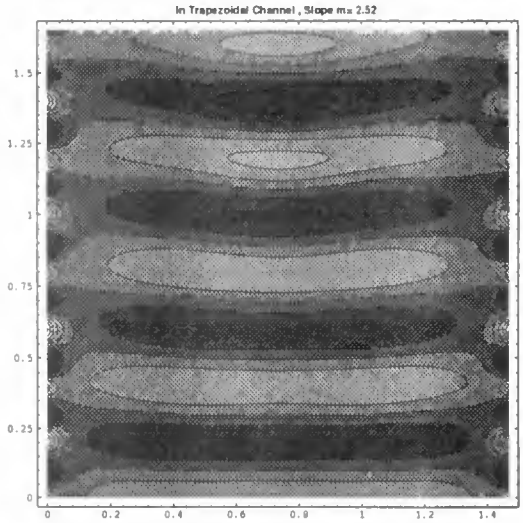

Figure 1: Plane View of Instantaneous Water Surface Elevation in Trapezoidal Channel Case 2; Ocean at the Bottom of Figure, Harbor to the Top. Edgewaves are excited at both the left and the right sides of the channel.

In this paper, a series of small scale laboratory experiments were conducted to verify the theoretical model. We studied the wave motion in triangular and trapezoidal channels with smooth sidewalls. Measurements of the free surface profile at different locations for several cross sections were obtained. The eigenfunctions were obtained from the wave displacement data by using Empirical Orthogonal Eigenfunction (EOF) method and were compared to those obtained from the numerical model.

2 Experiment Set-up

The wave experiments were conducted in a small tank at the Center of Applied Coastal Research at the University of Delaware. This section describes the experimental setup for the wave propagating in the channel and data acquisition procedure.

The tank was 236.0cm long, 122.5cm wide and 20.0cm deep. Waves were generated by a flap wavemaker at one end. Figures 2 and 3 show the experimental setup and tank. Two pieces of glass were used in the tank in order to form a triangular channel. Each piece of glass was 60.0cm wide, 165.0cm long and 0.64cm thick. Each glass panel was supported by two pieces of wood, allowing for the ability to vary the slopes of the sidewalls of the channel and to avoid any major deflection caused by bending. In order to diminish wave reflection, a gravel beach was located at the end of the tank. Four capacitance wave gages were used to measure the variations in the free surface.

Figure 3 shows the setup of the gages. Three gages were mounted on a movable fiberglass boom allowing for measurement at any particular position along the channel. The gages were numbered 1 through 4. Gage 4 in particular was placed parallel to the sloping side of channel and was used to measure the edge waves. Since the channel was symmetric in cross-section, gages were placed on only one side of the channel. In Figure 3, we define y as the horizontal coordinate taken to be positive landward, and $y = 0$ at the location of the midpoint of the channel cross-section.

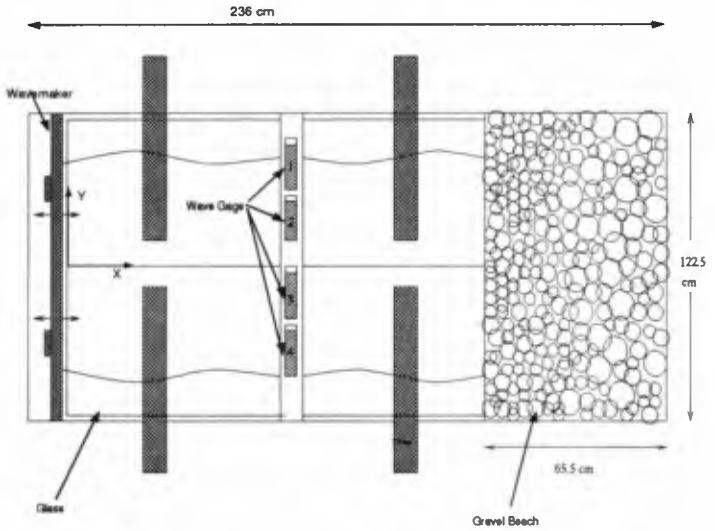

Figure 2: Experimental Setup (Top View)

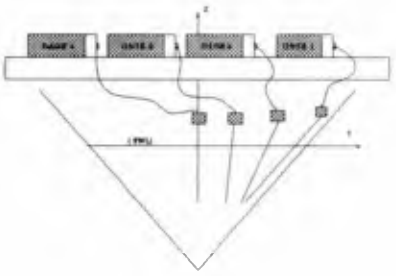

Figure 3: Layout of Wave Gages across Triangular Channel (Side View)

2.1 Analysis of Wave Data

Four tests, exploring the effect of varying channel slopes and varying wave frequencies for triangular channels, were conducted, as listed in Table 1.

Table 1: List of Experiments with Triangular Channel

Test	Slope	Wave Period (s)	Water Depth (m)	Measurement Locations	
				Along Channel Distance from Wavemaker d_x (m)	Across Channel Distance from Center point d_y (m)
S1F1	1:2.9	0.700	0.0705	0.950	0.030 0.070 0.120 0.195
S1F2	1:2.9	0.800	0.0705	0.985	0.030 0.070 0.120 0.195
S2F1	1:3.1	0.680	0.0650	0.985	0.015 0.050 0.100 0.190
S2F2	1:3.1	0.725	0.0650	0.950	0.015 0.050 0.100 0.190

Two additional tests were also performed for trapezoidal channel, varying the wave frequencies; as listed in Table 2.

Table 2: List of Experiments with Trapezoidal Channel

Test	Slope	Wave Period (s)	Water Depth (m)	Measurement Locations	
				Along Channel Distance from Wavemaker d_x (m)	Across Channel Distance from Center point d_y (m)
S3P1	1:2.5	0.570	0.0675	0.680	0.120 0.245 0.367 0.450 0.512 0.565 0.625 0.730
S3P2	1:2.5	0.570	0.0675	1.095	0.120 0.245 0.367 0.450 0.512 0.565 0.625 0.730

In order to test the repeatability of the experiments, each test was repeated six times. Test data from the six cases, including the time series and the amplitudes of the free surface waves were used for the data analysis. The eigenfunctions of the wave form across the channel were computed by the EOF method and later compared to the numerical model solution. The contour plots of the instantaneous wave field for the triangular and trapezoidal channels are also shown later.

3 Experimental Results

3.1 Comparison of Numerical Model To Experimental Data for Surface Profile

The amplitude of the propagating wave measured by each gage was used to create a surface profile along channel cross section. The amplitude η^i is defined by the mean maximum magnitude of time series for each gage:

$$\eta^i = \overline{\max(\eta^i(t))}$$

The surface profiles for the numerical solution and the experimental data are shown in Figures 4 through 9 (by symmetry, only half of the channel is shown; solid line indicates results of the numerical solution and the dot marks mean experimental data). The group of dots on the far right, are the experimental data obtained from the measure point close to the shoreline, representing the maximum magnitudes of the edge wave. The group of dots on the far left, are the experimental data obtained from the measuring point near the center line of channel, which represents the maximum magnitudes of the incident wave. The measuring error along y distance is $\pm 0.0018m$. As shown in these figures, there is a good agreement between the experimental data and numerical solution. The edge wave amplitude, represented by the zeroth mode eigenfunction, is much higher than the magnitude of the incident wave.

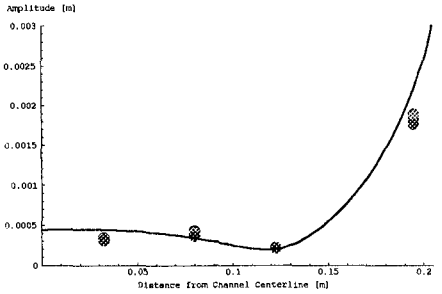

Figure 4: Comparison between the Cross-Channel Free Surface Profile for Case S1F1 and Numerical Solution, T=0.700 s, 0.950 m from Wavemaker

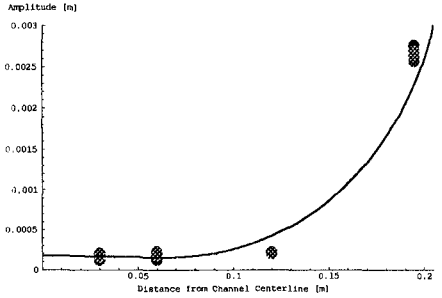

Figure 5: Comparison between the Cross-Channel Free Surface Profile for Case S1F2 and Numerical Solution, T=0.800 s, 0.985 m from Wavemaker

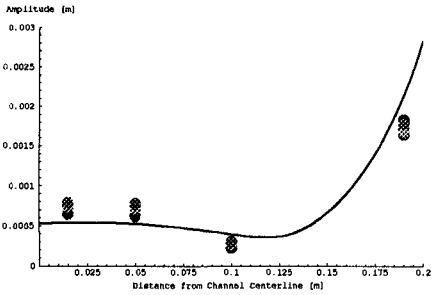

Figure 6: Comparison between the Cross-Channel Free Surface Profile for Case S2F1 and Numerical Solution, T=0.680 s, 0.985 m from Wavemaker

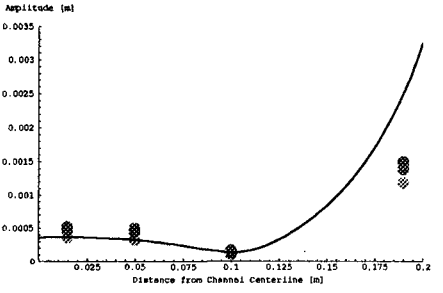

Figure 7: Comparison between the Cross-Channel Free Surface Profile for Case S2F2 and Numerical Solution, T=0.725 s, 0.950 m from Wavemaker

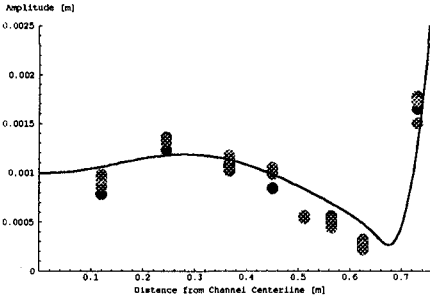

Figure 8: Comparison between the Cross-Channel Free Surface Profile for Case S3P1 and Numerical Solution, 0.680 m from Wavemaker

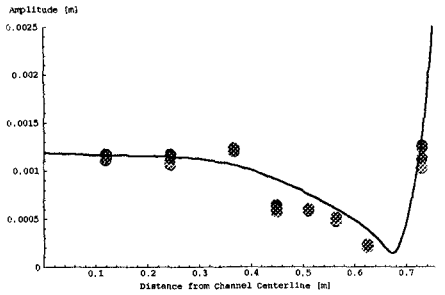

Figure 9: Comparison between the Cross-Channel Free Surface Profile for Case S3P2 and Numerical Solution, 1.095 m from Wavemaker

3.2 Comparison of Eigenfunction from Numerical Model and Experiment

3.2.1 The EOF method

The surface profile is assumed to be a superposition of eigenfunctions. Eigenfunctions can be obtained from the experimental data by using EOF(Empirical Orthogonal Eigenfunction) method.

The EOF method is a widely-used statistical tool which has been used for a number of analyses, including beach profile analysis. For the surface wave profile, the theoretical basis of the EOF method is the same as that for beach profile. The first eigenfunction is selected so that it accounts for the greatest possible amount of the data variance (the variance is defined as the mean square of the free surface displacement). The successive eigenfunctions each in turn are selected such that they represent the greatest possible amount of the remaining variance, Winant, Inman and Nordstrom (1975, as cited in Dean and Dalrymple, 1995).

The free surface displacement time series are recorded at the same time at the I locations across the channel width. Assume that there are K data points in one free surface displacement time series. These measured elevation are denoted as η_{ik}.

$$\eta_{ik} = \sum_{n=1}^{N} C_{nk} e_{ni}$$

for each I positions. Here, e_{ni} represents the n^{th} empirical eigenfunction evaluated at the i^{th} location across the channel width; and the constant C_{nk} represents a coefficient for the k^{th} recorded data and the n^{th} eigenfunction.

One property of the eigenfunctions is that they are independent of each other and orthogonal; that is,

$$\sum_{i=1}^{I} e_{ni} e_{mi} = \delta_{nm}$$

where $\delta_{nm} = 1$ if $n = m$, and it is zero otherwise. To obtain the value of the unknown C_{nk}, the error is mininized in the fit of η_{ik} by the eigenfunction. The minimization is carried out in the least squares sense by

$$2\sum_{i=1}^{I}(\eta_{ik} - \sum_{n=1}^{N} C_{nk} e_{ni}) e_m i = 0$$

Using the orthogonality relationship,

$$C_{mk} = \sum_{i=1}^{I} \eta_{ik} e_{mi}$$

Parseval's theorem is then applied: the sum of the squares of the coefficients is equal to the square of the variance. To find each eigenfunction, its contribution to the variance will be maximized. Finally, by using the Lagrange Multiplier approach, the following equation can be obtained

$$a_{im} = \frac{1}{IK} \sum_{k=1}^{K} \eta_{ik} \eta_{mk}$$

and the symmetric matrix equation

$$\sum_{i=1}^{I} a_{im} e_{ni} = \lambda e_{nm} \tag{1}$$

Equation 1 is an eigenvalue matrix equation, consisting of a symmetric real coefficient matrix. By solving this matrix equation, eigenfunctions are obtained as many as measured locations I in the cross-section of channel. The eigenfunctions obtained by EOF method from experimental free surface displacement time series are discussed in next section.

3.2.2 Comparison of Eigenfunction from Numerical Model and Experiment

The zeroth mode eigenfunction for the trapezoidal channel obtained from the experiment by the EOF method is compared to that obtained from numerical solution, as shown in Figures 10 through 13. From the numerical model, amplitude of the zeroth mode edge wave is normalized to unity. The next eigenmode has a magnitude of 0.32. The third mode has an amplitude of only 0.18. From the experiment by the EOF method, the maximum amplitude of the zeroth mode eigenfunction is 1.0. The next eigenmode has the maximum magnitude of 0.067. The third mode has an amplitude of only 0.037. From both methods, it is clearly seen that the wave motion can be viewed as a summation of simple eigenfunctions, and the zeroth mode eigenfunction is the dominant one.

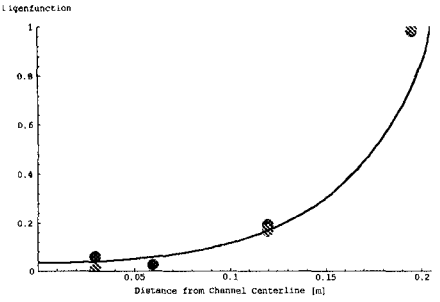

Figure 10: Comparison between the Zeroth Mode Eigenfunction for Case S1F2 and Numerical Solution, slope=1:2.9, T=0.800 s, h=0.0705 m, 0.985 m from Wavemaker

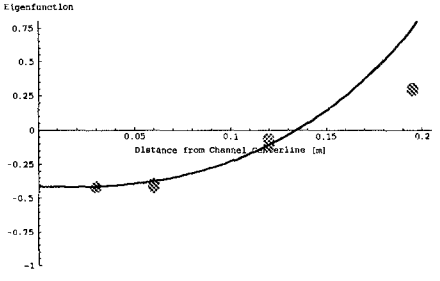

Figure 11: Comparison between the First Mode Eigenfunction for Case S1F2 and Numerical Solution

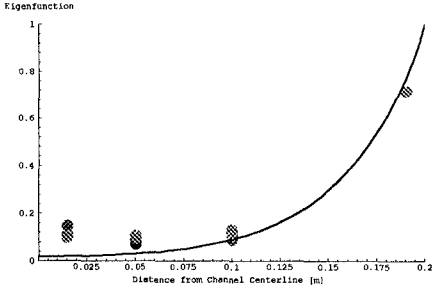

Figure 12: Comparison between the Zeroth Mode Eigenfunction for Case S2F2 and Numerical Solution, slope=1:3.1, T=0.725 s, h=0.0650 m, 0.950 m from Wavemaker

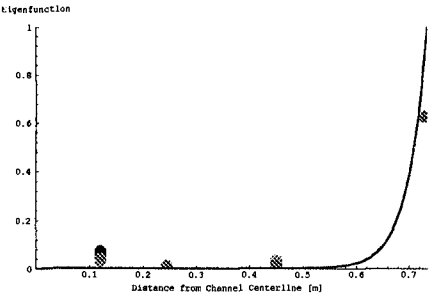

Figure 13: Comparison between the Zeroth Mode Eigenfunction for Trapezoidal Channel and Numerical Solution, slope=1:2.5, T=0.570 s, h=0.0675 m, 0.680 m from Wavemaker

3.3 Resonance ?

Figure 1 shows the instantaneous wave field obtained by the numerical model for the trapezoidal channel used in the test. It shows that zeroth mode edge wave has a wave length half of the incident wave length. From the nonlinear wave theory, the second harmonic wave over a flat bottom has a wave length equal to half of that of the incident wave. The issue whether there is any relationship between the zero mode edge wave and the second harmonic wave will be discussed will be discussed here. Typical wave spectra in the experiments for trapezoidal channel are shown in Figures 14 and 15, which indicate the second harmonic wave frequency is twice of the first harmonic wave frequency.

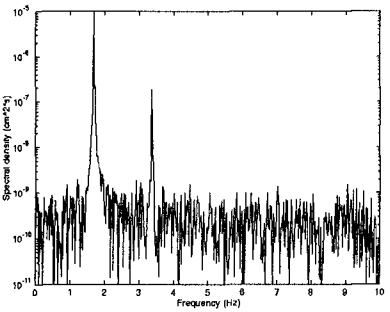

Figure 14: Wave Spectrum from Wave Data at Point: 0.410 m from Wavemaker, 0.425 m from Channel Center Line

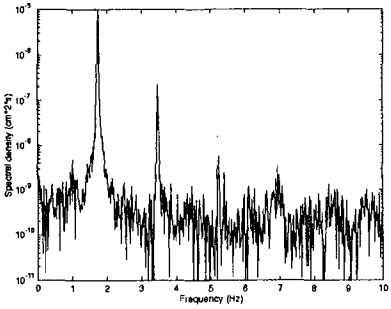

Figure 15: Wave Spectrum from Wave Data at Point: 0.820 m from Wavemaker, 0.425 m from Channel Center Line

Figure 16 shows the amplitude of the first three harmonics down the trapezoidal channel along the center line of the half-channel width, and Figure 17 shows the amplitude of the first three harmonics down the trapezoidal channel along the shoreline of the channel. It is seen that the second harmonics does not increase as might be expected by nonlinear interactions with the wave in the channel providing the forcing for edge wave growth (as indicated before). So the edge wave does not exhibit any resonance with the second harmonic of the incident wave.

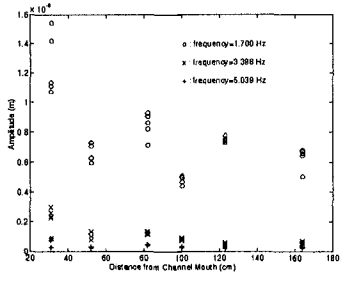

Figure 16: The Amplitudes of The First Three Harmonics Down the Channel; Channel Mouth to the Left, Channel End to the Right

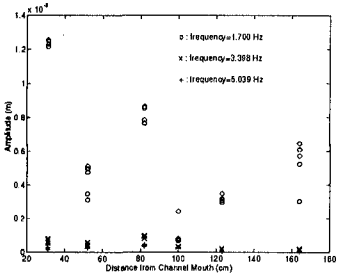

Figure 17: The Amplitudes of The First Three Harmonics Down the Channel along the Sidewall

4 Conclusion

A series of small scale laboratory experiments for triangular channel and trapezoidal channel were conducted to provide substance to the theoretical argument. It shows the experimental data exhibit good agreement with the numerical solutions.The results from the experiments and the numerical model show that channels with sloping sidewalls give rise to the presence of edge waves, excited by the incident wave field, while the incident wave propagate in the center of channel. The edge wave length is shorter than the incident wave length. The edge wave amplitude, represented by the zeroth mode eigenfunction, is much higher than the magnitude of the incident wave. According to the weight of each eigenfunction, the edge wave modes are the dominant ones in the wave motion. Because the amplitudes of higher harmonics do not increase, the edge wave does not exhibit any resonance with the second harmonic of the incident wave.

Reference

Dalrymple, R.A. (1989), "Water Waves Past Abrupt Channel Transitions," *Applied Ocean Research*, v. 11, n. 4, pp 170-175.

Dalrymple, R.A. (1992), "Water Wave Propagation in Jettied Channels," *Proc. 23rd Intl. Conference on Coastal Engineering*, pp 3040–3053 .

Dalrymple, R.A. and J.T. Kirby (1988), "Models for Very Wide Angle Water Waves and Wave Diffraction," *Journal of Fluid Mechanics*, v. 192, pp 33-50.

Dalrymple, R.A. and J.T. Kirby (1992), "Angular Spectrum Modelling of Water Waves," *Reviews in Aquatic Sciences*, CRC Press, 6, Iss. 5 and 6, pp 383-404.

Dalrymple, R.A., J.T. Kirby and P.A. Martin (1994), "Spectral Methods for Forward-Propagating Water Waves in Conformally-Mapped Channels," *Applied Ocean Research*, v. 16, pp 249-266.

Dalrymple, R.A., J.T. Kirby and L. Li (1994), "The Propagation of Water Waves in Channels," *Proc. Intl. Symp. on Waves*, IAHR, Vancouver, pp 570-579.

Dalrymple, R.A. and P.A. Martin (1996), " Water Waves Incident on an Infinitely Long Rectangular Inlet," *Applied Ocean Research*, v. 18, pp 1-11.

Dean, R.G. and R.A. Dalrymple (1995), **Coastal Processes** *with Engineering Applications*, manuscript.

Golinko, V.I. (1987), "Interaction Between a Vertical Wall and a Wave Propagating in a Channel of Parabolic Cross Section", *Fluid Dyn.*, v. 22, n. 1, pp 87-90.

Isaacson, M. de St.Q. (1978), "Wave Damping Due to Rubblemound Breakwater," *J. Waterways, Port, Coastal and Ocean Division*, v. 104, WW4, pp 391-405.

Lamb, H. (1945), **Hydrodynamics**, 6^{th} ed., New York, Dover Press, 1945.

Mathew, J. and T.R. Akylas (1990), "On Three-Dimensional Long Water Waves in a Channel with Sloping Sidewalls", *J. Fluid Mech.*, v. 215, pp 289-307.

Melo, E. and R.T. Guza (1991a), "Wave Propagation in a Jettied Entrance Channel, I: Models," *J. Waterways, Port, Coastal and Ocean Engrg.*, v. 117, n. 5, pp 471–492.

Melo, E. and R.T. Guza (1991b), "Wave Propagation in a Jettied Entrance Channel, II: Observations," *J. Waterways, Port, Coastal and Ocean Engrg.*, v. 117, n. 5, pp 493–510.

Peregrine, D.H. (1968), "Long Waves in a Uniform Channel of Arbitrary Cross-Section", *J. Fluid Mechanics*, v. 32, pp 353-365.

Peregrine, D.H. (1969), "Solitary Waves in Trapezoidal Channel", *J. Fluid Mechanics*, v. 35, pp 1-6.

Teng, M.H. and T.Y. Wu (1994), "Evolution of Long Water Waves in Variable Channels", *Journal of Fluid Mechanics*, v. 266, pp 303-317.

Winant, C.D., D.L. Inman and C.E. Nordstrom (1975), "Description of Seasonal Beach Changes using Empirical Eigenfunction," *J. Geophy. Res.*, 80, 15, pp 1976-1986.